

The Abundance of Molecular Hydrogen and its Correlation with Midplane Pressure in Galaxies: Non-Equilibrium, Turbulent, Chemical Models

Mordecai-Mark Mac Low^{1,2} & Simon C. O. Glover²

¹*Department of Astrophysics, American Museum of Natural History,
Central Park West at 79th Street, New York, NY 10024*

²*Zentrum der Astrophysik der Universität Heidelberg, Institut für Theoretische Astrophysik,
Albert-Ueberle-Straße 2, 69120 Heidelberg, Germany*

mordecai@amnh.org, glover@uni-heidelberg.de

ABSTRACT

Observations of spiral galaxies show a strong linear correlation between the ratio of molecular to atomic hydrogen surface density R_{mol} and midplane pressure. To explain this, we simulate three-dimensional, magnetized turbulence, including simplified treatments of non-equilibrium chemistry and the propagation of dissociating radiation, to follow the formation of H_2 from cold atomic gas. The formation time scale for H_2 is sufficiently long that equilibrium is not reached within the 20–30 Myr lifetimes of molecular clouds. The equilibrium balance between radiative dissociation and H_2 formation on dust grains fails to predict the time-dependent molecular fractions we find. A simple, time-dependent model of H_2 formation can reproduce the gross behavior, although turbulent density perturbations increase molecular fractions by a factor of few above it. In contradiction to equilibrium models, radiative dissociation of molecules plays little role in our model for diffuse radiation fields with strengths less than ten times that of the solar neighborhood, because of the effective self-shielding of H_2 . The observed correlation of R_{mol} with pressure corresponds to a correlation with local gas density if the effective temperature in the cold neutral medium of galactic disks is roughly constant. We indeed find such a correlation of R_{mol} with density. If we examine the value of R_{mol} in our local models after a free-fall time at their average density, as expected for models of molecular cloud formation by large-scale gravitational instability, our models reproduce the observed correlation over more than an order of magnitude range in density.

Subject headings: astrochemistry — molecular processes — ISM: molecules — ISM: clouds

1. Introduction

Stars are universally observed to form in molecular clouds. Indeed, recent observations have demonstrated that the surface density of star formation Σ_{SFR} correlates linearly with the surface density of molecular hydrogen Σ_{H_2} (Rownd & Young 1999; Wong & Blitz 2002; Gao & Solomon 2004; Bigiel et al. 2008, 2011). This has led to the suspicion that the formation of stars depends on the formation of molecular hydrogen (Schaye 2004; Krumholz & McKee 2005; Elmegreen 2007; Krumholz et al. 2009b). However, the opposite view has also been argued: that molecular clouds and then stars form from converging flows (Ballesteros-Paredes et al. 1999; Koyama & Inutsuka 2000; Hartmann et al. 2001; Vázquez-Semadeni et al. 2006; Ballesteros-Paredes et al. 2007; Hennebelle et al. 2008; Heitsch & Hartmann 2008; Inoue & Inutsuka 2009), primarily driven by large-scale gravitational instability (Rafikov 2001; Kim & Ostriker 2001; Elmegreen 2002; Kravtsov 2003; Dalcanton et al. 2004; Mac Low & Klessen 2004; Li et al. 2005, 2006; Shetty & Ostriker 2008; Ostriker et al. 2010). In this picture, the formation of molecules is a consequence, not a cause, of the conditions required to form stars.

Wong & Blitz (2002) and Blitz & Rosolowsky (2004, 2006) added to the puzzle with the observation that in the inner parts of spiral galaxies the ratio of molecular to atomic hydrogen surface density

$$R_{\text{mol}} \equiv \Sigma_{\text{H}_2}/\Sigma_{\text{HI}} \propto P_m, \quad (1)$$

where P_m is the midplane pressure and Σ_{HI} is the surface density of H I. In detail, they derived an empirical pressure dependence for R_{mol} that can be fit several different ways. Taking a common fit to all their individual data points yields the fit (Blitz & Rosolowsky 2006)

$$R_{\text{mol}} = \left[\frac{P_m/k}{(4.5 \pm 0.14) \times 10^4} \right]^{0.94 \pm 0.02}, \quad (2)$$

where P_m/k has units of K cm^{-3} . This result was extended by Leroy et al. (2008) who studied a broad sample of spiral and dwarf galaxies from THINGS, and gave the results in their Table 6. They found results quite consistent with equation (2).

Both Blitz & Rosolowsky (2006) and Krumholz et al. (2009a) offered explanations of this observed correlation that rely on the equilibrium balance between radiative dissociation and H_2 molecule formation on the surfaces of dust grains. Blitz & Rosolowsky (2006) built on the original suggestion by Elmegreen (1989) and Elmegreen & Parravano (1994) that the midplane pressure in disk galaxies determines molecular cloud properties. They began with the calculation by Elmegreen (1993) that the equilibrium fraction of gas in the molecular phase

$$f_{\text{mol}} \equiv \Sigma_{\text{H}_2}/\Sigma_{\text{tot}} \quad (3)$$

depends on both the interstellar pressure and the radiation field j as

$$f_{\text{mol}} \propto P_m^{2.2} j^{-1}. \quad (4)$$

This equation was derived by assuming two populations of spherical clouds, one with constant density, representing diffuse clouds, and one with r^{-2} density profiles, representing hydrostatic, self-gravitating clouds. Observations (Heiles 2001) and turbulent models (de Avillez & Breitschwerdt 2005; Joung & Mac Low 2006; Glover et al. 2010) reveal that the distribution of densities among the diffuse clouds is continuous rather than the delta functions predicted by thermal phase transitions, demonstrating some of the limitations of this approach.

For low values of $R_{\text{mol}} \lesssim 0.5$, the approximation $R_{\text{mol}} \simeq f_{\text{mol}}$ can be made. Blitz & Rosolowsky (2006) then invoked the observed correlation $\Sigma_{\text{SFR}} \propto \Sigma_{\text{H}_2}$, and assumed that the star formation rate determines the local radiation field directly ($j \propto \Sigma_{\text{SFR}}$) to derive that

$$R_{\text{mol}} \propto P_m^{1.2}. \quad (5)$$

However, the discussion in Blitz & Rosolowsky (2006) and Leroy et al. (2008) neglects that this relationship does not hold for the high values of $R_{\text{mol}} \gg 0.5$ observed in some galaxies, as Equation (4) does not hold, nor does the approximation $R_{\text{mol}} \simeq f_{\text{mol}}$.

Krumholz et al. (2009a,b), and McKee & Krumholz (2010) calculate the equilibrium value of f_{mol} in a uniform-density, spherical gas cloud exposed to far ultraviolet (FUV) radiation. An essentially identical result was already derived for a slab model of a cloud by Sternberg (1988). They all demonstrate that the fraction depends on only two parameters. The first parameter is the characteristic dust optical depth $\tau_R = n_H \sigma_d R$ of a cloud of radius R , where n_H is the number density of hydrogen nuclei in the atomic gas, and σ_d is the cross section for dust absorption per hydrogen atom. The second parameter is the effective intensity of the ionizing radiation

$$\chi = f_d \sigma_d c E_0^* / (n_H \mathcal{R}), \quad (6)$$

(denoted αG by Sternberg 1988), where f_d is the fraction of absorbed photons in the Lyman-Werner bands that result in dissociation, $c E_0^*$ is the ambient flux of radiation in the Lyman-Werner bands, and \mathcal{R} is the rate coefficient for the formation of H_2 on grains.

The effective intensity χ can be written in terms of the value of G'_0 , the ratio of E_0^* to the typical dissociating radiation field in the Milky way of $G_0 = 7.5 \times 10^{-4}$ photons $\text{cm}^{-2} \text{s}^{-1}$ (Draine 1978), as

$$\chi = 71 (\sigma_{d,-21} / \mathcal{R}_{-16.5}) (G'_0 / n_H), \quad (7)$$

where $\sigma_{d,-21} = \sigma_d/10^{-21} \text{ cm}^{-2}$ and $\mathcal{R}_{-16.5} = \mathcal{R}/10^{-16.5} \text{ cm}^3 \text{ s}^{-1}$. Both scaled constants are of order unity in the solar neighborhood. Krumholz et al. (2009b) and McKee & Krumholz (2010) go on to express χ in terms of the metallicity and the physical constants only, by assuming that the atomic gas is in two-phase thermal equilibrium. However, this second step is not required. Not taking it allows application of their chemical model to a cloud of arbitrary density and ambient radiation field.

These two papers then extend their approximation to compute f_{mol} in a spherical cloud composed of both atomic and molecular gas, by making the assumption that the atomic gas is in pressure equilibrium with the colder, denser molecular gas. This allows them to derive a fit to f_{mol} for the spherical gas cloud as a function solely of χ , Σ_{tot} , the dust cross section σ_d , and the mean mass per hydrogen nucleus μ_H . Using the improved approximation given by McKee & Krumholz (2010),

$$f_{\text{mol}} \approx 1 + \left(\frac{3}{4}\right) \frac{s}{1 + s/4}, \quad (8)$$

for $s < 2$, where,

$$s = \ln(1 + 0.6\chi + 0.01\chi^2)/(0.6\tau_c), \quad (9)$$

and the optical depth through the atomic-molecular cloud $\tau_c = 0.75\Sigma_{\text{tot}}\sigma_d/\mu_H$. For $s > 2$, $f_{\text{mol}} = 0$ is a better approximation. Essentially this same relationship was used by Krumholz et al. (2009b) to derive the star formation rate in galaxies, taking into account the observed correlation between molecular hydrogen and star formation surface density.

But why should H_2 exert such a strong influence on star formation? Although H_2 is a coolant, it is effective only down to temperatures of 200 K, whereas atomic fine structure emission (primarily from C^+) can cool the gas down to temperatures of around 60 K in regions of low dust extinction, or as low as 15 K in more highly shielded regions where the photoelectric heating rate is small (Glover & Mac Low 2007b; Glover & Clark 2011). To cool further, to the 10 K typical of most prestellar cores, generally requires CO, which indeed forms efficiently only in H_2 -rich gas. However, the difference between 20 K and 10 K can only slightly affect the star formation rate, as demonstrated by the recent simulations of Glover & Clark (2011).

On the other hand, gravitational instability produces dense gas that quickly forms H_2 (Glover & Mac Low 2007b). Thus, H_2 , and other molecules that form with it, such as CO, may primarily just act to trace dense gas that is already gravitationally unstable and collapsing. Ostriker et al. (2010) present an analytic model for how the combination of dynamical and thermal equilibrium may lead to this situation, also yielding a prediction of the correlation between the molecular surface density and the midplane pressure based on the

linear relation derived between radiation field strength and pressure. However, this model relies on the empirical correlation $\Sigma_{\text{SFR}} \propto \Sigma_{\text{H}_2}$ without offering a theoretical explanation for it.

In this paper we examine the evolution of the molecular hydrogen to atomic hydrogen ratio R_{mol} as a function of time and examine whether that evolution can explain its observed correlation with pressure, and thus its relationship to the star formation rate. To do this, we have incorporated a simplified, non-equilibrium, chemical network and radiative transfer model into a three-dimensional simulation of supersonic (and super-Alfvénic), magnetohydrodynamical turbulence. This allows us to follow the formation history of H_2 , starting from turbulent, magnetized atomic gas (Glover & Mac Low 2007a; Glover et al. 2010).

Our models follow the interplay between the cold neutral medium (CNM) and molecular gas at different average densities. They have velocity dispersions of 5 km s^{-1} , with resulting densities dispersed around the mean value by more than four orders of magnitude (see Fig. 7 of Glover et al. 2010). Although we do not explicitly model gravitational collapse, we do examine regions with varying average density, providing a first approximation to the sequence of quasi-static states that a large-scale, gravitationally contracting region will pass through. Only a small fraction of the molecular gas will ever undergo full-scale gravitational collapse (Goldreich & Kwan 1974; Krumholz & Tan 2007), with the rest remaining at pressures close to the surrounding atomic gas. Because we do include the full suite of heating and cooling processes relevant for both cold atomic and molecular gas, our models offer insight into the behavior of the cold gas even on large scales.

At any particular time after molecules begin forming, we find that the molecular fraction R_{mol} varies primarily as a function of local gas volume density, almost independently of radiation field strength, except in diffuse regions with mean extinctions of $A_V \lesssim 0.3$. This is because the strong self-shielding of H_2 means the rate-limiting step in denser regions is the slow formation of molecules on dust grains. Significant mass fractions of the flow in these models become fully molecular in only a few million years (Glover & Mac Low 2007b), but molecule formation continues over periods exceeding 20 Myr, comparable to cloud lifetimes. Thus, equilibrium values of the molecular fraction cannot be relied on. This is contrary to the behavior of CO, whose fractional abundance is far more sensitive to the dust column density (and thus radiation field strength) than to the volume density, because of its much weaker ability to self-shield (Glover & Mac Low 2011).

If molecular clouds rarely or never reach equilibrium, then what determines the observed molecular fraction? The hypothesis that global star formation is controlled by gravitational instability of the gaseous disk has been considered at least since the calculation of the gravitational instability criterion in such disks by Goldreich & Lynden-Bell (1965). Numerical

simulations by Kravtsov (2003); Li et al. (2006), and Tasker & Bryan (2006) supported this idea, demonstrating that it naturally could explain observations of both global (Kennicutt 1998) and local (Martin & Kennicutt 2001; Bigiel et al. 2008) correlations between gas surface density and star formation rate. The clumpy nature of high-redshift galaxies can also be explained by this hypothesis (Bournaud et al. 2007; Bournaud & Elmegreen 2009). Molecular cloud formation as a by product of gravitational instability has been argued to be a natural consequence of this hypothesis (Elmegreen 2002; Mac Low & Klessen 2004; Li et al. 2005; Ballesteros-Paredes et al. 2007; Tasker & Tan 2009). This suggests that the key timescale is the free-fall time

$$t_{\text{ff}} = (G\rho)^{-1/2}, \quad (10)$$

at the local average density $\rho = \langle \mu_H n_H \rangle$. We show that our non-equilibrium models indeed predict the observed molecular fractions to occur after a free-fall time at the average density in each model.

In section 2 we describe our numerical method and the models that we ran. We then offer a simple analytical model of molecular hydrogen formation in section 3 and discuss how it succeeds and fails in comparison to the full numerical results. In section 4 we compare our results to equilibrium models and the observations, while in section 5 we offer caveats and consider the implications of our results.

2. Numerical Method

To study the formation of molecular hydrogen from atomic hydrogen, we use mesoscale simulations of turbulent, magnetized, atomic gas incorporating a non-equilibrium chemical network, including an approximation to the background dissociating radiation field. In order to resolve the turbulent flow sufficiently well to follow the formation of H_2 , we neglect the large scale structure of the interstellar medium, and instead simulate periodic boxes with side length $L = 5\text{--}20$ pc having defined average initial number density n_0 (and other parameters such as metallicity Z , turbulent velocity dispersion, and magnetic flux).

We use a version of ZEUS-MP (Hayes et al. 2006) modified to include a subcycled chemical model and the associated radiative and chemical heating and cooling. The method was described in detail in Glover et al. (2010) but for the models presented here we explore a wider range of initial conditions and run several of the simulations for considerably longer. Radiative transfer is included using a six-ray approximation, with column densities measured from the edges of the cube (Glover & Mac Low 2007a). Although this is not strictly self-consistent, it does capture the basic dynamics of radiative dissociation well (also see Glover et al. 2010 and Glover & Mac Low 2011).

All of the models presented here include driven turbulence, rather than the decaying turbulence used in Glover & Mac Low (2007b), with an rms velocity $v_{rms} = 5 \text{ km s}^{-1}$, and an initial vertical magnetic field of $B_0 = 5.85 \mu\text{G}$. In Table 1 we give the initial density n_0 and metallicity Z , the box size L , the strength of the radiation field G in units of G_0 , and the number of zones along one edge of the cube nx .

3. Molecule Formation

Our models show that the molecular to atomic ratio R_{mol} grows almost as a power law in time over many dynamical times (Figure 1). Although our models will eventually reach saturation, the time taken to do so is generally longer than the plausible lifetimes for molecular clouds of 20–30 Myr (Fukui & Kawamura 2010). We only find evidence for reaching an equilibrium value of R_{mol} within the first 25 Myr of evolution of our models for the model with the least active molecule formation (the low density and metallicity model n30-Z01 discussed in § 4.1).

3.1. Formation Time

We can derive a simple analytic model for the behavior seen in our simulations by considering the finite formation timescale of molecular hydrogen in a uniform medium. A rather similar approach is followed by Gnedin et al. (2009). The fractional local density of molecular hydrogen

$$X_{\text{H}_2} = 2n_{\text{H}_2}/n, \quad (11)$$

where $n = n_{\text{H}} + 2n_{\text{H}_2}$, grows as

$$\dot{X}_{\text{H}_2} = C(t)n_{\text{H}}\mathcal{R}(T), \quad (12)$$

where the formation rate $\mathcal{R} \propto T^{1/2}$, and we have included a time dependent clumping factor C to account for the density perturbations. We can eliminate n_{H} from these two equations to find

$$\dot{X}_{\text{H}_2} = 2Cn_{\text{H}_2}\mathcal{R}(1/X_{\text{H}_2} - 1). \quad (13)$$

Integrating this equation with a change of variable and the assumption of a uniform value for the clumping factor C , we find

$$X_{\text{H}_2} = 1 - \exp(-t/\tau_F), \quad (14)$$

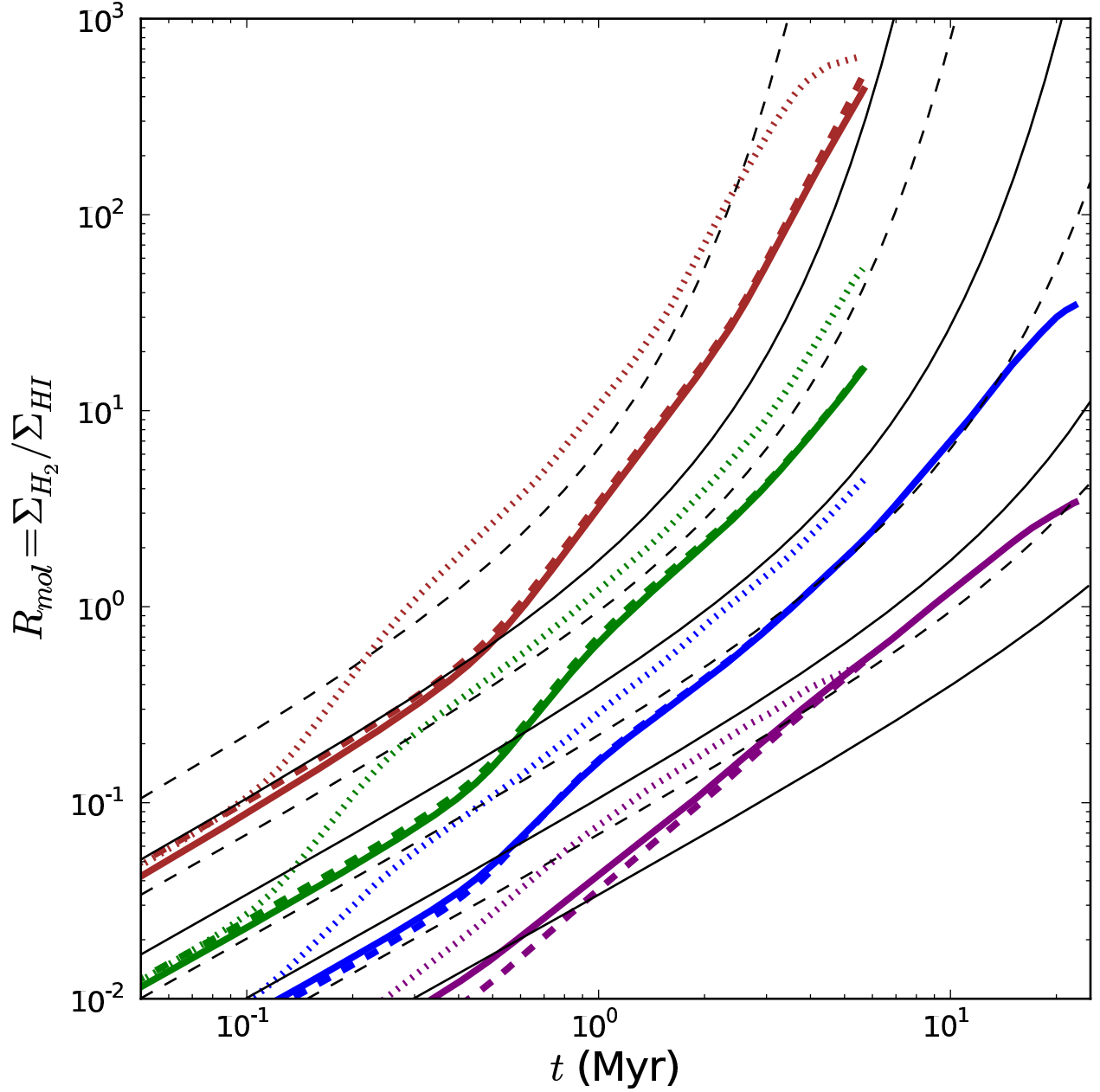


Fig. 1.— Time history of the value of the column density ratio R_{mol} integrated through turbulent, magnetized boxes, starting with purely atomic gas, for models listed in Table 1. Models shown have average number density 30 (*purple, lowest*), 100 (*blue*), 300 (*green*), and 1000 (*brown, highest*) cm^{-3} . Canonical models (*solid*) are compared with G0 models lacking radiation (*dashed*), and -L5 models with smaller boxes (*dotted*). The thin, solid, black curves show the analytic model given by Equation (14) for time constants given by Equation (15) for the densities of each model, while the thin, dashed, black curves show the analytic model with a clumping factor of two. The small box models diverge from the unclumped predictions earlier, as expected. No single clumping factor exactly reproduces all results.

where $\tau_F = 1/(C\mathcal{R}n)$ is the time constant for H_2 formation. Hollenbach & McKee (1979) already showed that for typical molecular cloud temperatures and without clumping ($C = 1$),

$$\tau_F \simeq \frac{1 \text{ Gyr}}{n/(1 \text{ cm}^{-3})}. \quad (15)$$

The assumption of no clumping should be good for times much less than the dynamical time $t_{\text{dyn}} = L/v_{\text{rms}}$, when the average density rather than the peak clump density determines the evolution. In our canonical model, $t_{\text{dyn}} = 3.9 \text{ Myr}$, while our small box models with suffix L5 have $t_{\text{dyn}} = 0.98 \text{ Myr}$.

We can compare this simple model with our numerical results and the observations under the assumption that the local density ratio X_{H_2} can be used to derive the column density ratio $R_{\text{mol}} = X_{\text{H}_2}/(1 - X_{\text{H}_2})$. Figure 1 shows that, as expected, this analytic model works well at early times, up to roughly 0.4 Myr for the canonical model, and 0.1 Myr for our small box models. In both cases, this represents a clumping time

$$\delta t_c \sim 0.1 t_{\text{dyn}}. \quad (16)$$

Thereafter, R_{mol} increases above the prediction of the simplest model, because of the enhanced clumping caused by the turbulence (Glover & Mac Low 2007b).

3.2. Clumping

The assumption of an equilibrium fraction of molecular hydrogen fails, not just because of the long formation timescale of molecular hydrogen but also because molecular hydrogen does not form uniformly. Supersonic turbulence in the cold, neutral, atomic medium produces strong, transient, density perturbations. Peak densities exceed the average value by the square of the local thermal Mach number, which for conditions in the cold neutral medium can be a factor of $\delta n/n > 25$. Since the formation timescale (Eq. 14) is inversely proportional to density, formation proceeds far more quickly in the density peaks. Because of the strong self-shielding of H_2 , it does not immediately photodissociate when it subsequently advects into lower density regions, leading to non-equilibrium fractions in lower density regions (Glover & Mac Low 2007b).

No constant value of the clumping factor fits the late time results, however. For example, the value of $C = 2$ used in Figure 1 fits the $n = 30 \text{ cm}^{-3}$ results well at late time, but overpredicts the canonical $n = 1000 \text{ cm}^{-3}$ result substantially, though it does match the small box model well at late times. The time and density dependent variation of the clumping factor has begun to be studied by Milosavljevic et al. (2011).

4. Comparisons

4.1. Equilibrium Models

We compare a selection of our time-dependent results for turbulent gas to the equilibrium values derived for spherical clouds by McKee & Krumholz (2010). In Figure 2 we compare time histories of a representative set of our models to the approximate equilibrium values of R_{mol} for the conditions of each of these models given by Equation (8), taking Σ_{tot} to be the column density through the cubical simulation domain, and $R_{\text{mol}} = f_{\text{mol}}/(1 - f_{\text{mol}})$. The equilibrium approximation works particularly poorly at $R_{\text{mol}} \ll 1$, predicting no molecules in many cases where we find measurable molecular fractions. At larger values of R_{mol} , our models do intersect the spherical, equilibrium values, but at widely varied times, and with no indication of asymptotic approach to those values.

The equilibrium models predict strong variation depending on the ambient radiation field, while we see little to no effect (comparing the G0 and G10 models to the canonical models, we see that they are practically identical in the n300 case). This is because the evolution is controlled by H_2 formation rather than photodissociation equilibrium. This occurs because the supersonic turbulent flows have strong density enhancements, leading both to efficient self-shielding in the regions where most H_2 is forming and also fast local molecule growth in those enhancements.

We do note that the equilibrium models in the intermediate regime give the qualitatively correct result of H_2 formation at moderate densities. Although this is neither quantitatively correct nor extendible to other regimes, it nevertheless means that observational comparisons that rely only on this qualitative result can be successfully made to the equilibrium models.

The value of R_{mol} in our models depends on the metallicity, through its regulation of the dust density, and thus the H_2 formation rate. However, only our very lowest density and metallicity model n30-Z01 approaches an equilibrium value during the 20 Myr that we ran our models. This suggests that real molecular clouds rarely find themselves in equilibrium with the diffuse radiation field because their lifetimes are not long enough (Fukui & Kawamura 2010). Instead, they are probably dissociated and dispersed by intense, local, UV radiation from newly formed stars.

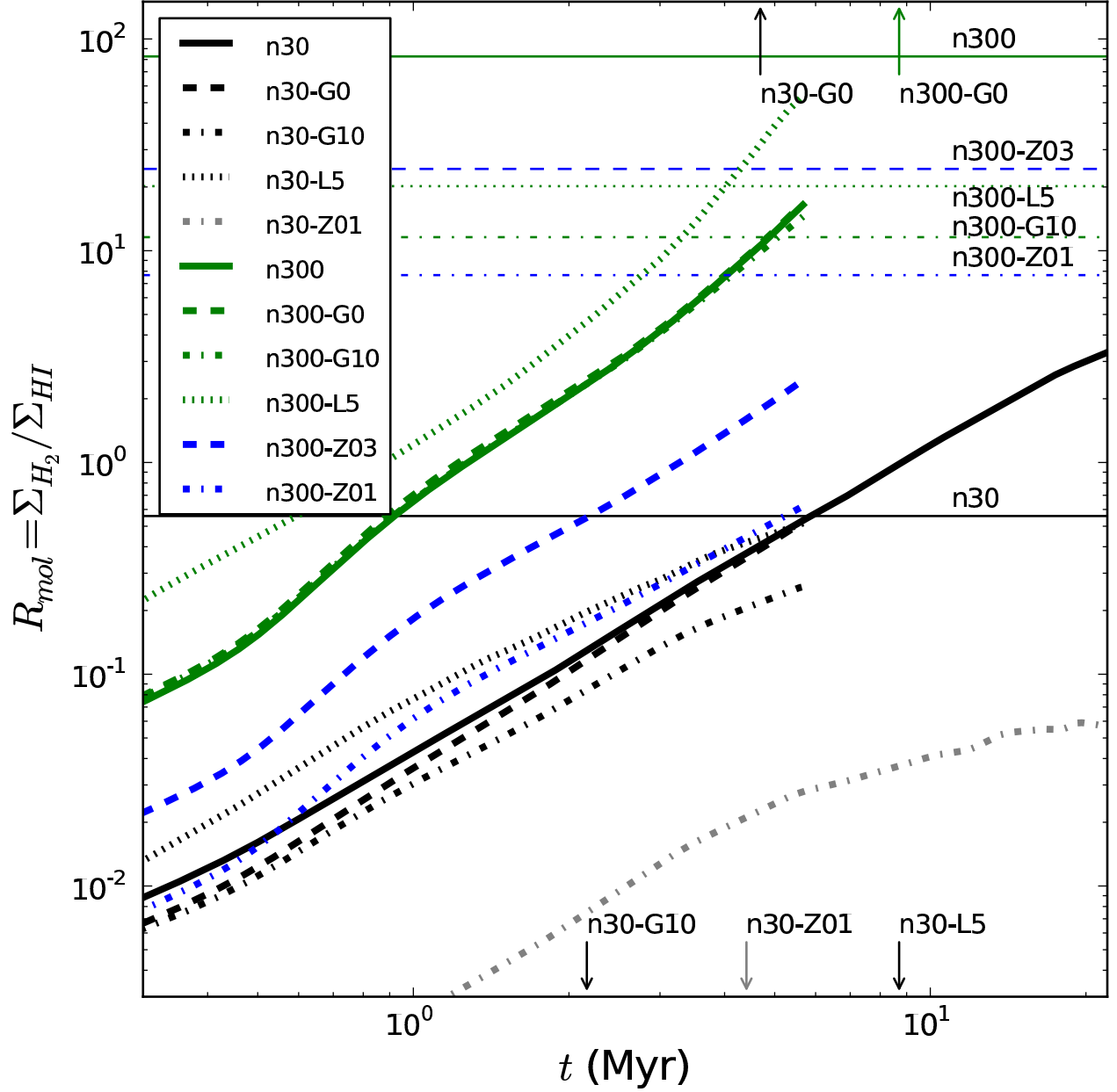


Fig. 2.— Time history of R_{mol} for models with average number density 30 (black, grey), and 300 (green, blue) cm^{-3} . Canonical models (solid) are compared with G0 models lacking radiation (dashed), G10 models with ten times higher radiation (dash-dotted), L5 models with smaller boxes (dotted), and low metallicity models with 0.3 (blue dot-dashed) and 0.1 (blue, grey dashed) the canonical metallicity. The models with varying levels of radiation in the high density case almost entirely overlap each other. Thin horizontal lines and arrows show the predictions from the equilibrium calculation described by McKee & Krumholz (2010) as given in Equation (8). The predictions for the radiation-free G0 models are $R_{\text{mol}} \rightarrow \infty$, while the high-radiation, low-density case, as well as a number of other models, is predicted to have $R_{\text{mol}} = 0$, as indicated by the arrows at the top and bottom of the plot. The very weak dependence of our models on radiation strength directly contradicts the prediction of the equilibrium models.

4.2. Observations

Averaged over kiloparsec scales, the average temperature, magnetic pressure, and turbulent velocity dispersion of the cold, neutral medium vary little, with $T_{CNM} \sim 60\text{--}70\text{K}$ (Wolfire et al. 1995, 2003), field strength $B \sim 5\mu\text{G}$ (Heiles & Troland 2003) or perhaps 20% higher as seen in observations of external galaxies (Beck 2005), and turbulent Mach number $M_t \sim 5$ (Heiles & Troland 2003). Ostriker et al. (2010) argue that this roughly constant effective dynamical temperature comes from self-regulation of star formation. The roughly constant dynamical temperature suggests that the apparent dependence of the fraction R_{mol} on pressure P_m given in Equation (2) may actually reflect a density dependence, as already suggested by Blitz & Rosolowsky (2004).

Figure 1 indeed shows a clear density dependence, but it also shows strong time dependence, raising the question of what molecular fraction should actually be compared with the observations. If the hypothesis holds that molecular clouds actually form during large-scale gravitational instability as discussed in § 1, then the characteristic time in their lives at which clouds will be observed is a free-fall time (Eq. 10) after gravitational collapse begins in cooled atomic gas. Our models do not begin with clumped atomic gas as the actual ISM does. Instead, the turbulent flows initialized on the grid clump the gas over a finite time δt_c (Eq. 16). In order to account for this effect, we have taken the zero point in time for this comparison to be δt_c rather than the initial time of our models. We emphasize that the observations show an order of magnitude scatter around the average $R_{\text{mol}}\text{--}P_m$ correlation, so that using a characteristic time to describe a time-dependent process appears likely to be consistent with the observations if they catch clouds at different points in their evolution centered around a free-fall time.

Each of our models has a fixed average density n_H given in Table 1. We use that value to compute the average pressure in our models

$$P = n_H k T_{CNM} + \langle B^2 \rangle / 8\pi + 0.5 \mu_H n_H v_{rms}^2, \quad (17)$$

where we assume that $T_{CNM} = 60\text{ K}$, and the mean mass per particle $\mu_H = 2.11 \times 10^{-24}$ appropriate for atomic gas with 10% helium by number. Because our models are subject to dynamo generation of magnetic field from the initial value, we use the actual values of the average magnetic pressure at each time rather than the initial value.

We then use Equation (2) to derive the value and standard deviation of R_{mol} predicted by Blitz & Rosolowsky (2006) for the pressure for that model by setting $P_m = P$. We also derive values of R_{mol} from the spiral and dwarf samples of Leroy et al. (2008). The spiral sample has $R_{\text{mol}} = (10^{-4.23} P_m / k)^{0.80}$, while the dwarf sample has $R_{\text{mol}} = (10^{-4.51} P_m / k)^{1.05}$. All of these values are plotted in Figure 3 at times $t_{\text{ff}}(n_H)$ after the beginning of evolution

of our models.

We find that our models predict the observed R_{mol} across more than an order of magnitude in pressure, with an accuracy better than the scatter in the observationally derived relations themselves. The ability to predict not just a single value, but a whole family of values accurately suggests that we have captured the important physics of the variation of the molecular fraction R_{mol} with the estimated midplane pressure.

5. Discussion

5.1. Influence of numerical resolution

Figure 3 shows that the values of R_{mol} we find in our $L = 5$ pc simulations are systematically higher at late times than those found in our $L = 20$ pc simulations. (This is in addition to the early time differences discussed above that occur because of the difference in crossing time t_{dyn} between the two box sizes.) Since both sets of runs were performed with the same numerical resolution of $nx = 128$ zones per side, the spatial resolution of our L5 runs is four times larger than that in our other runs. This prompts the concern that our simulations may be under-resolved, and that our reported results for R_{mol} might have a significant dependence on the spatial resolution of the simulations.

To investigate this, we have performed several additional simulations with a higher numerical resolution. In Figure 4(a), we compare the evolution of R_{mol} in two canonical runs and the corresponding L5 runs, with that in two runs performed using the same sets of simulation parameters, but with twice the numerical resolution. Increasing the resolution to $nx = 256$ zones per side leads to slightly faster production of H_2 at late times, particularly in the lower density runs, since we are better able to resolve the highest density structures produced by the turbulence. However, the effect is small, and does not explain the significantly larger difference that we see between the results of the 5 pc (L5) and 20 pc runs.

Ideally, we would perform a similar comparison using results from runs with $L = 20$ pc and a numerical resolution of 512^3 zones, which would have the same spatial resolution as our $L = 5$ pc runs. Unfortunately, the high computational cost of performing a 512^3 simulation using the full Glover et al. (2010) cooling and chemistry model has so far rendered this impractical.

However, it has been possible to perform simulations with this resolution by adopting a simpler treatment of the CO chemistry based on Nelson & Langer (1999). By using this simpler treatment, we accept a slightly higher degree of error in our predicted CO, C and

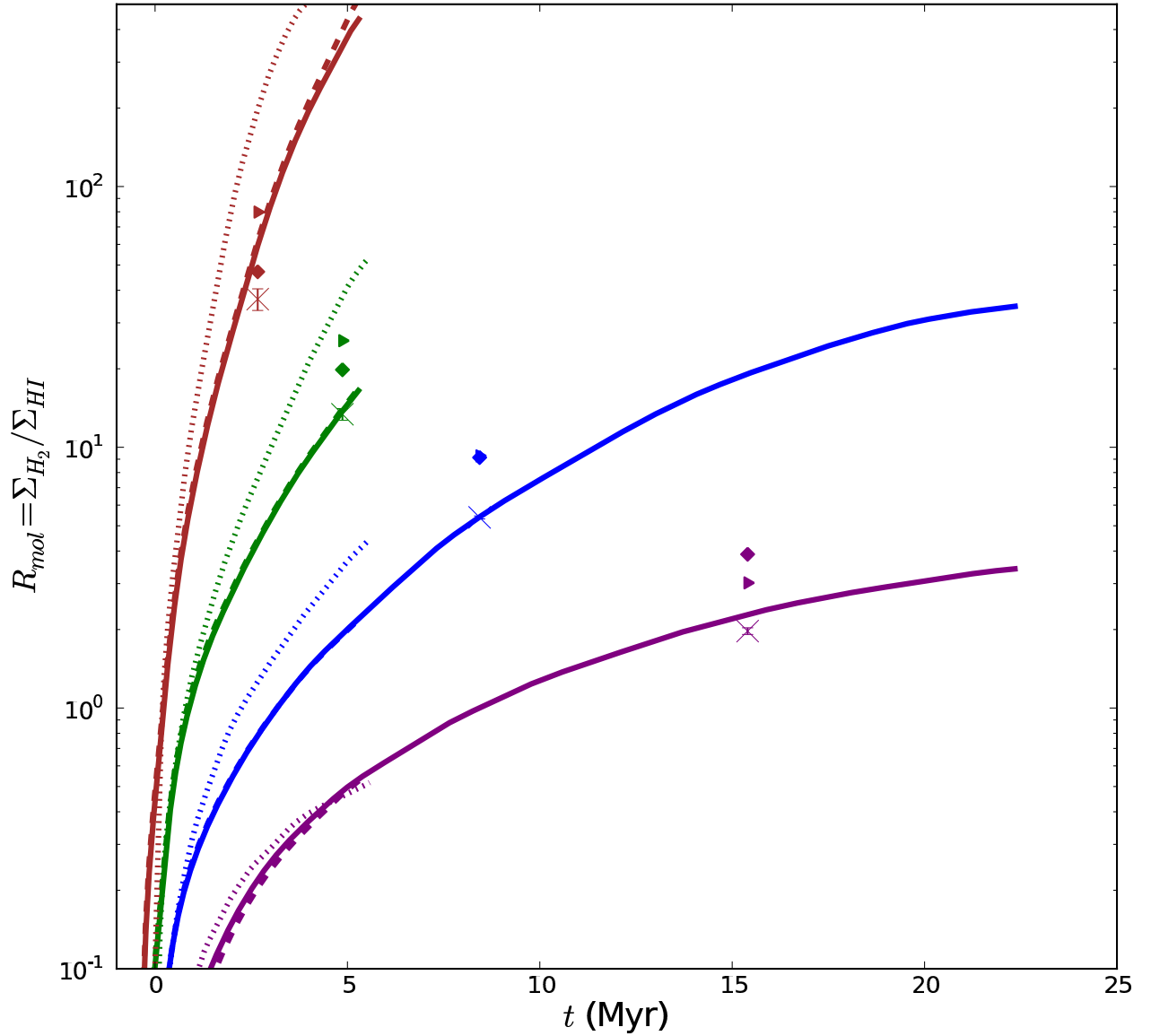


Fig. 3.— Time history of the value of the column density ratio R_{mol} for the same models presented in Figure 1, shown on semi-log axes for clarity. Superposed, we show the empirical fit for the canonical model of each density of Blitz & Rosolowsky (2006), including the errors (X), as well as the spiral (*diamond*) and dwarf (*triangle*) galaxy samples of Leroy et al. (2008). For all points we take a CNM temperature of 60 K, and the average density, time-dependent magnetic pressure, and turbulent pressure of each model. They are placed on the figure at a free-fall time for the average density of that model, as described in the text. To account for clumping of the atomic ISM, we use a zero time of δt_c in this plot, so that the initial time of each model is negative.

C^+ abundances, and lose our ability to follow the evolution of chemical species such as OH or water, but still retain the ability to follow the evolution of the H_2 abundance accurately, since our treatment of the hydrogen chemistry remains the same. At these densities, the change in cooling from the modified chemistry will produce negligible changes in the chemical evolution. We show the results of this full resolution study in Figure 4(b). Once again, we see that although our results remain somewhat sensitive to the numerical resolution of the simulation, the effect is relatively small and cannot be responsible for the difference between the $L = 5$ pc and $L = 20$ pc runs.

If spatial resolution is not the answer, then what is responsible for the difference between the runs with different box sizes at late times? The lower visual extinction of the gas in the smaller box allows stronger photoelectric heating, which leads to the gas in the L5 runs having a systematically higher temperature than the gas in the larger volume simulations. For example, the volume weighted mean temperature of the gas at the end of run n300 is approximately 40 K, while in run n300-L5 it is 66 K. This difference in temperatures leads to a systematic difference in the H_2 formation rate coefficient, owing to the $T^{1/2}$ temperature dependence of the rate coefficient, and hence leads to a faster production of H_2 in the smaller volume simulations.

5.2. Caveats

In this section, we discuss the limitations of this work. The biggest problem is that we are substituting a study of local isotropic turbulent regions without explicit self-gravity for one of the dynamical interstellar medium. However, to reach the resolutions of less than 0.2 pc used here in any large-scale model of the interstellar medium remains computationally challenging. These resolutions are required in order to resolve the turbulent density peaks that determine the H_2 formation rate.

We approximate the external field of FUV dissociating radiation by injecting radiation at the boundaries of our periodic box. Although this is physically inconsistent, we find that in this study it makes virtually no difference, as models with and without FUV behave almost identically. This is because the densities that we study are sufficiently high that H_2 self-shielding efficiently blocks penetration of UV into the dense regions where H_2 forms and remains. This also means that the opening of voids in the density distribution by the turbulence has much less effect on the H_2 fraction than the creation of density peaks.

In our models, we do not include local sources of dissociating or ionizing radiation. Star formation of course produces such local sources, which can be effective at dispersing molec-

ular clouds on short time scales. Turbulent models of such dispersal have not yet been performed, but analytic models assuming spherical symmetry by Matzner (2002) and Elmegreen (2007) show that large clouds can be dispersed in a dynamical time. Similarly, analytic models including accretion show lifetimes comparable to the observed values of around 20 Myr (Fukui & Kawamura 2010) in either a slab converging flow (Zamora-Aviles & Vázquez-Semadeni 2011) or a spherical geometry (Goldbaum et al. 2011). These relatively short cloud destruction time scales support our assumption that most clouds are observed at an age of roughly a free-fall time.

Our chemical model has been simplified to allow computation on a three-dimensional grid. However, in the range of temperatures and densities considered here, Glover et al. (2010) have shown that we reproduce the results of the UMIST model to within a few tens of percent. Moreover, we do not expect any of the chemical processes omitted from the model to have a significant impact on the fractional abundance of molecular hydrogen, and hence our values for R_{mol} should be quite accurate.

Finally, we assume in this study that the dominant contributions to the observed column densities of atomic and molecular hydrogen come from cold, dense clouds, rather than from the warm, diffuse medium surrounding these clouds. This is good to better than a factor of two in the Milky Way where cold gas represents roughly $6M_{\odot} \text{ pc}^{-2}$ while warm atomic and ionized gas is a bit less than $5M_{\odot} \text{ pc}^{-2}$ (Ferrière 2001), and is probably better in more massive disks, but will break down in outer disks or other regions where the WNM component dominates the mass budget. Since in practice R_{mol} is only measured in regions where CO emission can be detected, our approximation should be reasonable in the regime where observations are available.

5.3. Comparison to Other Tests

Krumholz & Gnedin (2011) tested the equilibrium models of Krumholz et al. (2009b) (see eq. 8) against relatively low-resolution (smallest zone size $\Delta x = 65 \text{ pc}$) global numerical simulations of H_2 formation in galaxies. The simulations were described by Gnedin & Kravtsov (2010), and used the H_2 formation law of Gnedin et al. (2009). Krumholz & Gnedin (2011) found good agreement in cases where we find that our models reach high molecular fractions quickly (those with high density and low radiation intensity), but poor agreement in cases where we find that time-dependence matters. The formation law of Gnedin et al. (2009) effectively reproduces the simple model that we have described in Equation (14). The inability of global models to resolve the density peaks is captured in the higher value of the clumping factor they require to reproduce observations. Because lower mean densities are deduced,

these models do still overestimate the sensitivity of molecule formation to radiation.

Fumagalli et al. (2010) compared the equilibrium model given by Equation (8) to local (100 pc beam size) observations of the column density of H I and global (1 kpc beam size) observations of CO and H I. They demonstrate that the equilibrium model with freely adjusted clumping factor predicts high molecular fractions in regions of high local density, as we also predict without such an adjustable factor, and that there is a metallicity dependence, again as we also predict.

5.4. Implications for the Star Formation Rate in Galaxies

We have demonstrated that the molecular fraction R_{mol} remains strongly time dependent over periods of rather more than 20 Myr (Fig. 1). Our high-resolution numerical results provide calibration for the time-dependent molecule formation model of Gnedin et al. (2009) which assumes similar physics, but must rely on much larger clumping factors to reproduce sub-grid scale turbulence. Equilibrium values of R_{mol} are only reached at times well beyond the lifetimes of real molecular clouds of 20–30 Myr (Fukui & Kawamura 2010). Therefore, explanations of the observed correlation between midplane pressure and R_{mol} that rely on equilibrium values seem unlikely to be correct.

We find that the observed correlation can nevertheless be explained if most molecular gas occurs in regions that have been forming H_2 for a free-fall time at their current number density (Fig. 3). This is a natural prediction for the gravitational instability model for star formation in galaxies. Molecular cloud formation occurs as part of the same process of large scale collapse that eventually forms stars, so the observed correlation between molecular hydrogen and star formation rate surface densities comes about because they have a common cause, not because the first controls the second.

Our result appears almost independent of the strength of the far ultraviolet dissociating radiation field during formation of the molecular clouds, as can be seen by the close agreement of our canonical models with otherwise identical models run without or with stronger dissociating radiation. In future work the upper limits of this behavior must be examined, since clearly a strong enough radiation field will eventually dissociate molecular gas, or at least ionize enough of it to dynamically disperse it, allowing dissociation to occur. In particular, once massive star formation begins, the intense local radiation field probably does dissociate or disperse the remaining molecular hydrogen, terminating molecule formation relatively quickly and determining the cloud lifetime.

The metallicity clearly influences the molecular hydrogen formation rate in our mod-

els, through its regulation of the dust density (Fig. 2). The H_2 formation rate depends on the product nZ of the number density and the metallicity (Glover & Mac Low 2011) because of the role of dust grains in the formation reaction, so this is expected. However, we find a weaker sensitivity than suggested by Equation (8) derived from an equilibrium model. Detailed comparison of our results to galaxies with varying metallicity should prove informative.

We thank A. Leroy, E. Rosolowsky, & L. Blitz for insight into their data, and M. Krumholz, C. McKee, & B. Elmegreen for useful discussions. The clarity and emphasis of the revised version benefited from comments by the anonymous referee and M.-Y. Lee. M-MML was partly supported by NASA/SAO grant TM0-11008X, by NASA/STScI grant HST-AR-11780.02-A, and by NSF grants AST 08-06558 and AST 11-09395. SCOG acknowledges support from DFG grants KL1358/4 and KL1358/5, from a Heidelberg University Frontier Grant, funded as part of the German Excellence Initiative, from the Bundesministerium für Bildung und Forschung via the ASTRONET project STAR FORMAT (grant 05A09VHA), and from the Baden-Württemberg Stiftung via their program International Collaboration II (grant PLS-SPII/18). The numerical simulations discussed in this work were performed on the *kolob* cluster at Heidelberg University, and on the *Ranger* supercomputer at the Texas Advanced Computing Center, the latter under NSF Teragrid allocation TG-MCA99S024.

REFERENCES

- de Avillez, M. A., & Breitschwerdt, D. 2005, *A&A*, 436, 585
- Ballesteros-Paredes, J., Hartmann, L., & Vázquez-Semadeni, E. 1999, *ApJ*, 527, 285
- Ballesteros-Paredes, J., Klessen, R. S., Mac Low, M.-M., & Vázquez-Semadeni, E. 2007, in *Protostars and Planets V*, ed. B. Reipurth, D. Jewitt, and K. Keil (Tucson: University of Arizona Press), 63
- Beck, R. 2005, in *Cosmic Magnetic Fields*, ed. R. Wiełebinski, R. Beck (Berlin: Springer), 41
- Bigiel, F., Leroy, A., Walter, F., Brinks, E., de Blok, W. J. G., Madore, B., & Thornley, M. D. 2008, *AJ*, 136, 2846
- Bigiel, F., et al. 2011, *ApJ*, 730, L13
- Blitz, L., & Rosolowsky, E. 2006, *ApJ*, 650, 933

- Blitz, L., & Rosolowsky, E. 2004, *ApJ*, 612, L29
- Bournaud, F., Elmegreen, B. G., & Elmegreen, D. M. 2007, *ApJ*, 670, 237
- Bournaud, F., & Elmegreen, B. G. 2009, *ApJ*, 694, L158
- Brown, P. N., Byrne, G. D., & Hindmarsh, A. C. 1989, *SIAM J. Sci. Stat. Comput.*, 10, 1038
- Dalcanton, J. J., Yoachim, P., & Bernstein, R. A. 2004, *ApJ*, 608, 189
- Draine, B. T. 1978, *ApJS*, 36, 595
- Elmegreen, B. G. 1989, *ApJ*, 338, 178
- Elmegreen, B. G. 1993, *ApJ*, 411, 170
- Elmegreen, B. G. 2002, *ApJ*, 577, 206
- Elmegreen, B. G. 2007, *ApJ*, 668, 1064
- Elmegreen, B. G., & Parravano, A. 1994, *ApJ*, 435, L121
- Ferrière, K. M. 2001, *Rev. Mod. Phys.*, 73, 1031
- Fukui, Y., & Kawamura, A. 2010, *ARA&A*, 48, 547
- Fumagalli, M., Krumholz, M. R., & Hunt, L. K. 2010, *ApJ*, 722, 919
- Gao, Y., & Solomon, P. M. 2004, *ApJ*, 606, 271
- Glover, S. C. O., Federrath, C., Mac Low, M.-M., & Klessen, R. S. 2010, *MNRAS*, 404, 2
- Glover, S. C. O., & Mac Low, M.-M. 2007a, *ApJS*, 169, 239
- Glover, S. C. O., & Mac Low, M.-M. 2007b, *ApJ*, 659, 1317
- Glover, S. C. O., & Clark, P. C., *MNRAS*, submitted (arXiv:1105.3073)
- Glover, S. C. O., & Mac Low, M.-M. 2011, *MNRAS*, 412, 337
- Gnedin, N. Y., & Kravtsov, A. V. 2010, *ApJ*, 714, 287
- Gnedin, N. Y., Tassis, K., & Kravtsov, A. V. 2009, *ApJ*, 697, 55
- Goldbaum, N. J., Krumholz, M. R., Matzner, C. D., & McKee, C. F. 2011, *ApJ*, in press (arXiv:1105.6097)

- Goldreich, P., & Kwan, J. 1974, *ApJ*, 189, 441
- Goldreich, P., & Lynden-Bell, D. 1965, *MNRAS*, 130, 97
- Hartmann, L., Ballesteros-Paredes, J., & Bergin, E. A. 2001, *ApJ*, 562, 852
- Hayes, J. C., Norman, M. L., Fiedler, R. A., Bordner, J. O., Li, P. S., Clark, S. E., ud-Doula, A., & Mac Low, M.-M. 2006, *ApJS*, 165, 188
- Heiles, C. 2001, *ApJ*, 551, L105
- Heiles, C., & Troland, T. H. 2003, *ApJ*, 586, 1067
- Heitsch, F., & Hartmann, L. 2008, *ApJ*, 689, 290
- Hennebelle, P., Banerjee, R., Vázquez-Semadeni, E., Klessen, R. S., & Audit, E. 2008, *A&A*, 486, L43
- Hollenbach, D., & McKee, C. F. 1979, *ApJS*, 41, 555
- Inoue, T., & Inutsuka, S.-i. 2009, *ApJ*, 704, 161
- Joung, M. K. R., & Mac Low, M.-M. 2006, *ApJ*, 653, 1266
- Kennicutt, R. C., Jr. 1998, *ApJ*, 498, 541
- Kim, W.-T., & Ostriker, E. C. 2001, *ApJ*, 559, 70
- Koyama, H., & Inutsuka, S.-I. 2000, *ApJ*, 532, 980
- Kennicutt, R. C., Jr. 1998, *ApJ*, 498, 541
- Kravtsov, A. V. 2003, *ApJ*, 590, L1
- Krumholz, M. R., & Gnedin, N. Y. 2011, *ApJ*, 729, 36
- Krumholz, M. R., & McKee, C. F. 2005, *ApJ*, 630, 250
- Krumholz, M. R., McKee, C. F., & Tumlinson, J. 2009a, *ApJ*, 693, 216
- Krumholz, M. R., McKee, C. F., & Tumlinson, J. 2009b, *ApJ*, 699, 850
- Krumholz, M. R., & Tan, J. C. 2007, *ApJ*, 654, 304
- Leroy, A. K., Walter, F., Brinks, E., Bigiel, F., de Blok, W. J. G., Madore, B., & Thornley, M. D. 2008, *AJ*, 136, 2782

- Li, Y., Mac Low, M.-M., & Klessen, R. S. 2005, *ApJ*, 626, 823
- Li, Y., Mac Low, M.-M., & Klessen, R. S. 2006, *ApJ*, 639, 879
- Mac Low, M.-M., & Klessen, R. S. 2004, *Rev. Mod. Phys.*, 76, 125
- Martin, C. L., & Kennicutt, R. C., Jr. 2001, *ApJ*, 555, 301
- Matzner, C. D. 2002, *ApJ*, 566, 302
- McKee, C. F., & Krumholz, M. R. 2010, *ApJ*, 709, 308
- Milosavljevic, M., Glover, S. C. O., Federrath, C., & Klessen, R. S. 2011, *MNRAS*, submitted (arXiv:1103.3056)
- Nelson, R. P., & Langer, W. D. 1999, *ApJ*, 524, 923
- Ostriker, E. C., McKee, C. F., & Leroy, A. K. 2010, *ApJ*, 721, 975
- Rafikov, R. R. 2001, *MNRAS*, 323, 445
- Shetty, R., & Ostriker, E. C. 2008, *ApJ*, 684, 978
- Rownd, B. K., & Young, J. S. 1999, *AJ*, 118, 670
- Schaye, J. 2004, *ApJ*, 609, 667
- Sternberg, A. 1988, *ApJ*, 332, 400
- Tasker, E. J., & Bryan, G. L. 2006, *ApJ*, 641, 878
- Tasker, E. J., & Tan, J. C. 2009, *ApJ*, 700, 358
- Vázquez-Semadeni, E., Ryu, D., Passot, T., González, R. F., & Gazol, A. 2006, *ApJ*, 643, 245
- Wolfire, M. G., Hollenbach, D., McKee, C. F., Tielens, A. G. G. M., & Bakes, E. L. O. 1995, *ApJ*, 443, 152
- Wong, T., & Blitz, L. 2002, *ApJ*, 569, 157
- Wolfire, M. G., Hollenbach, D., McKee, C. F., Tielens, A. G. G. M., & Bakes, E. L. O. 1995, *ApJ*, 443, 152
- Wolfire, M. G., McKee, C. F., Hollenbach, D., & Tielens, A. G. G. M. 2003, *ApJ*, 587, 278

Zamora-Aviles, M., & Vázquez-Semadeni, E. 2011, ApJ, submitted (arXiv:1105.4777)

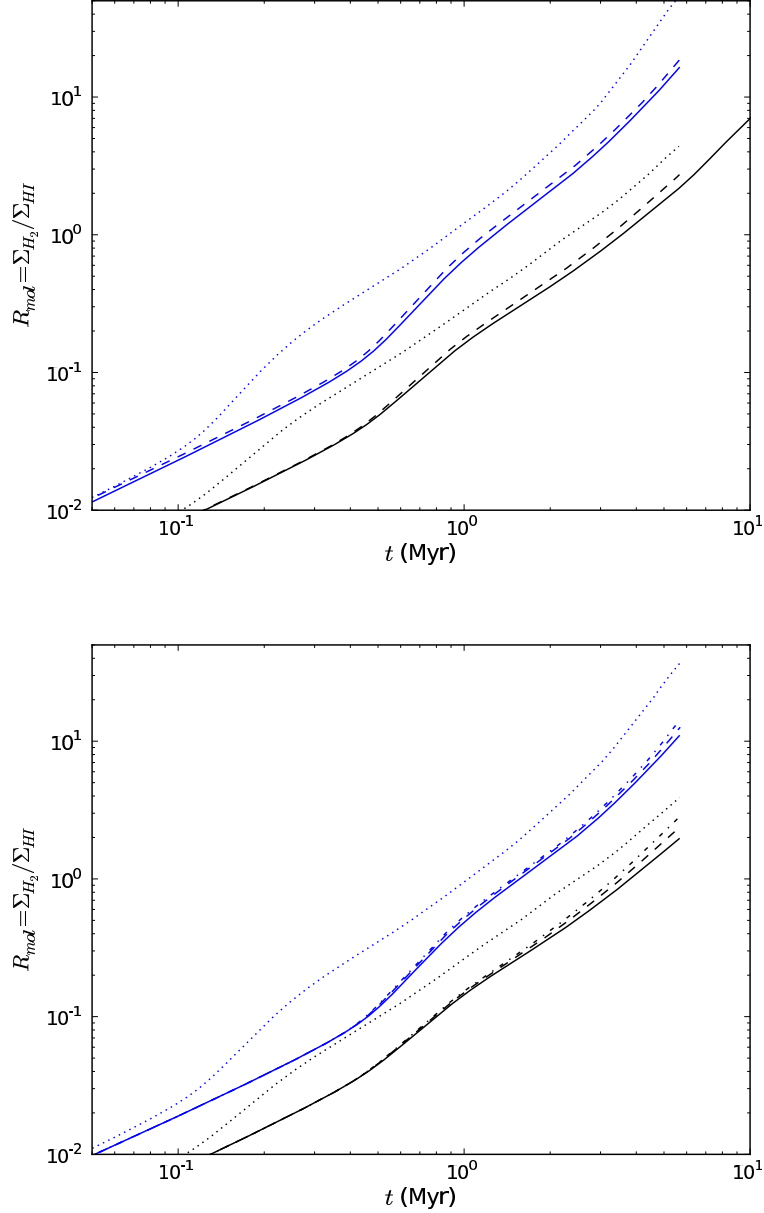


Fig. 4.— Resolution studies of the time history of R_{mol} . (a) Comparison of runs n100 (black, solid line) and n300 (blue, solid line) with runs n100-256 and n300-256 (dashed lines) having twice the numerical resolution, and with runs n100-L5 and n300-L5 (dotted lines), having four times the effective resolution but in a four times smaller box. (b) Resolution studies of the n100 (black) and n300 (blue) models reaching 512^3 resolution by using the reduced chemical network of Nelson & Langer (1999). Runs ending in NL-128 (solid lines), NL-256 (dashed lines), and NL-512 (dash-dotted lines) are directly compared to NL-L5 runs (dotted lines) that have physical resolution equivalent to the NL-512 runs.

Table 1. Input parameters used for each simulation.

Run	n_0 (cm^{-3})	Z (Z_\odot)	L (pc)	G (G_0)	nx (zones)
n30	30	1	20	1	128
n30-G0	30	1	20	0	128
n30-G10	30	1	20	10	128
n30-L5	30	1	5	1	128
n30-Z01	30	0.1	20	1	128
n100	100	1	20	1	128
n100-G0	100	1	20	0	128
n100-L5	100	1	5	1	128
n100-Z01	100	0.1	20	1	128
n100-256	100	1	20	1	256
n100-NL-128	100	1	20	1	128
n100-NL-256	100	1	20	1	256
n100-NL-512	100	1	20	1	512
n100-NL-L5	100	1	5	1	128
n300	300	1	20	1	128
n300-G0	300	1	20	0	128
n300-G10	300	1	20	10	128
n300-L5	300	1	5	1	128
n300-Z01	300	0.1	20	1	128
n300-Z03	300	0.3	20	1	128
n300-256	300	1	20	1	256
n300-NL-128	300	1	20	1	128
n300-NL-256	300	1	20	1	256
n300-NL-512	300	1	20	1	512
n300-NL-L5	300	1	5	1	128
n1000	1000	1	20	1	128
n1000-G0	1000	1	20	0	128
n1000-L5	1000	1	5	1	128

Note. — Z_{\odot} is the solar metallicity, while G_0 is the strength of the local interstellar radiation field as derived by Draine (1978). NL models were run without full carbon chemistry (see section 5.1).